International Journal of Modern Physics B
Vol. 32, No. 17 (2018) 1840020 (9 pages)

DOI: 10.1142/S0217979218400209

Structural and electronic response of overexpanded superconducting fullerides close to the Mott insulator boundary

M. Menelaou and Y. Takabayashi

WPI-Advanced Institute for Materials Research (WPI-AIMR), Tohoku University, Sendai 980-8577, Japan

H. E. Okur

WPI-Advanced Institute for Materials Research (WPI-AIMR), Tohoku University, Sendai 980-8577, Japan

Department of Chemistry, Bursa Technical University, Bursa 16310, Turkey

R. H. Zadik

Department of Chemistry, Durham University, Durham DH1 3LE, UK

K. Prassides*

WPI-Advanced Institute for Materials Research (WPI-AIMR), Tohoku University, Sendai 980-8577, Japan

**k.prassides@wpi-aimr.tohoku.ac.jp*

Accepted 7 February 2018
Published 15 March 2018

The ternary fulleride, $Rb_{0.25}Cs_{2.75}C_{60}$, is the most expanded member of the family of face-centered cubic (fcc) structured superconducting fullerides ever accessed with superconductivity surviving at ambient pressure closest to the Mott insulator boundary. Here, we study the evolution of its structural and electronic properties with temperature. At ambient temperature, $Rb_{0.25}Cs_{2.75}C_{60}$ lies in the Mott–Jahn–Teller (MJT) insulating part of the phase diagram. High-resolution synchrotron X-ray diffraction shows that its structure remains strictly cubic at all temperatures, but the transition to the metallic state at ~ 50 K — evident in the evolution of the magnetic susceptibility with temperature — is accompanied by a lattice collapse, $\Delta V/V_0$ of -0.5%. Bulk superconductivity then emerges on further cooling with a T_c of 25.9 K. The results permit the extension

*Corresponding author.

of the electronic phase diagram of A_3C_{60} fullerides as close as possible to the metal–insulator (M–I) crossover.

Keywords: Superconductivity; strong correlations; Mott insulator; insulator–metal transition; electronic phase diagram.

PACS numbers: 74.70.Wz, 71.30.+h, 74.62.Fj

1. Introduction

The understanding of high-temperature superconductivity in unconventional superconductors such as the cuprates is one of the greatest challenges in contemporary condensed matter physics.[1,2] The electronic phase diagrams of unconventional superconductors exhibit distinct commonalities in phase — superconductivity emerges from an antiferromagnetic strongly correlated Mott insulating state upon changing an external parameter such as doping or (physical/chemical) pressure and exhibits a dome-shaped dependence of the critical temperature, T_c.[3–5] Understanding how electron–electron interactions are controlled near the M–I crossover region is of generic significance for all strongly correlated systems and, in this regard, the study of the A_3C_{60} (A = alkali metal) molecular superconductors, in which fulleride frontier orbital degeneracy and geometrical frustration can be pressure-tuned[6–9] to access insulating, metallic, and superconducting states is of paramount importance. Contrary to long-held beliefs, fullerides have now been established as simple members of the unconventional superconductivity family, i.e., the pairing interaction is something other than simply the conventional BCS electron–phonon interaction.[6–21] Superconductivity in A_3C_{60} emerges upon applied (physical and/or chemical) pressure out of an antiferromagnetic Mott insulating state and displays an unconventional behavior — a superconductivity dome — explicable by the prominent role of strong electron correlations. In addition, there is a purely molecular aspect of the C_{60}^{3-} superconductivity story in that the parent insulating state involves Jahn–Teller distortion of the anion, driven by coupling of the localized t_{1u}^3 electrons to intramolecular phonons, thereby exemplifying the dominant role of the molecular electronic structure.[22,23] This on-molecule distortion is dynamic and creates an $S = 1/2$ ground state which produces the magnetism from which superconductivity emerges.

The striking similarities of the fulleride electronic phase diagram with those of high-T_c superconductors such as the cuprates also extend to the nature of the metallic state out of which both the insulator and superconductor emerge. The relation of this parent state to both the pairing mechanism and the proximate antiferromagnetic insulator is at the heart of any attempt to understand high-temperature unconventional superconductivity and has been feverishly pursued for decades in the cuprates.[24] The high symmetry and structural simplicity of the fullerides are here advantageous in pursuing a direct connection from (molecular) building unit to extended structure properties. By traversing the Mott insulator–metal transition in

the $Rb_xCs_{3-x}C_{60}$ ($0 \leq x \leq 3$) family of fullerides, an anomalous correlated metallic phase — the Jahn–Teller metal — was unveiled.[25] This state dominates the phase diagram at temperatures well above T_c and is the normal state at the maximum in T_c, where the superconducting pairing crosses over from conventional weak coupling to unconventional strong coupling. The Jahn–Teller metal is characterized by a dynamic, microscopically heterogeneous coexistence of itinerant metallic electrons with localized electrons, which produce on-molecule Jahn–Teller distortions.[25–27] This electronic state is the parent of an unconventional strongly-coupled superconductor and fades away into a conventional Fermi liquid metal and weak-coupling BCS superconductor as the molecular signatures disappear with lattice contraction. The optimal T_c in the fullerides — highest for any molecular material to date — associated with a strongly coupled (or extremely stable) Cooper pair and thus with an enhanced upper critical field as high as ~ 90 T is found at the boundary between unconventional and conventional behaviors,[28] where the balance between molecular (Jahn–Teller distortion) and extended lattice (itinerant electrons) features of the electronic structure is optimized.

In an attempt to access as close as possible the region of the electronic phase diagram bordering the Mott–Jahn–Teller (MJT) insulator from the metallic/superconducting side, we targeted the synthesis of $Rb_xCs_{3-x}C_{60}$ phases with x as close to 0 as possible while retaining ambient pressure superconducting response. We have now successfully synthesized the $Rb_{0.25}Cs_{2.75}C_{60}$ composition with an ambient pressure T_c of 25.9 K and report on the results of the investigation of the structural and electronic properties as the insulator-to-metal-to-superconductor transitions are traversed on cooling.

2. Experimental Procedures

2.1. *Synthesis and characterization*

The $Rb_{0.25}Cs_{2.75}C_{60}$ sample was prepared by a modification of the standard solid-state route, reported before,[25] to prepare ternary fullerides. Such a change in the synthetic protocol was necessary as when the Rb content approaches smaller and smaller values, phase separation is thermodynamically favored and the resulting materials contain only small fractions of the desired fcc-structured $Rb_xCs_{3-x}C_{60}$ product. Therefore, after an initial pre-treatment, the pelletized sample was first heated at 430°C for 15 h, and in contrast to the usual procedure of allowing it to cool in air, the sample was drop-quenched into liquid nitrogen. It was then reground, repelletized, and reheated at 430°C for an additional 52 h before being drop-quenched into an ice/salt water bath at $-1°$ to 2°C. This procedure successfully led to the enhancement of the phase fraction of the most expanded fcc-structured ambient pressure $Rb_{0.25}Cs_{2.75}C_{60}$ fulleride superconductor to as high as $\sim 80\%$ in the obtained material, as established by Rietveld analysis of powder X-ray diffraction data.

2.2. *Structural measurements*

High-resolution synchrotron X-ray diffraction experiments were carried out on the ID22 beamline at the European Synchrotron Radiation Facility (ESRF), France. The sample was sealed in a 0.5-mm diameter thin-wall glass capillary and diffraction profiles ($\lambda = 0.35420$ Å) were collected in continuous scanning mode at various temperatures between 15 and 300 K using a continuous-flow helium cryostat. The data were rebinned in the 2θ range 2–38° to a step of 0.003°. Analysis of the diffraction data was performed with the GSAS suite of Rietveld programs.[29]

2.3. *Magnetic measurements*

Ambient-pressure magnetic measurements of the $Rb_{0.25}Cs_{2.75}C_{60}$ composition were performed on a $\sim$21 mg sample sealed in a thin-walled quartz ampoule with a Quantum Design SQUID MPMS magnetometer. Temperature-dependent magnetic susceptibility, χ, data were collected at 3 and 5 T under field-cooled (FC) protocols at temperatures between 1.8 and 300 K. $\chi(T)$ was obtained from the difference of the values at 5 and 3 T in order to subtract out the contribution of ferromagnetic impurities evident in complementary field-dependent magnetization, M, data in applied fields between 0 and 5 T at 295 K. The magnetization, M, of the sample was also measured at an applied field of 10 Oe between 1.8 and 50 K under both zero-field cooled (ZFC) and FC protocols. Corrections for the diamagnetic core contributions of Rb^+, Cs^+, and C_{60}^{3-} ions (-0.225×10^{-4}, -0.35×10^{-4} and -2.43×10^{-4} emu mol^{-1}, respectively) were applied to all datasets.

3. Results and Discussion

Rietveld refinement of the synchrotron X-ray diffraction profile of the sample collected at 300 K confirmed the formation of a cubic phase with fcc symmetry (space group $Fm\bar{3}m$, $R_{wp} = 5.93\%$, $R_{exp} = 4.36\%$) and a lattice constant, $a = 14.71188(7)$ Å larger than those of any other $Rb_xCs_{3-x}C_{60}$ phase made before[25] but smaller than that of fcc-structured Cs_3C_{60}.[8] The fcc phase fraction in the sample is 78.14(4)% with the remaining comprising coexisting phases with composition CsC_{60} (11.3(3)%) and Cs_4C_{60}(10.5(2)%). The evolution of the diffraction profiles on cooling readily reveals that the cubic structure is robust and survives to 15 K, the lowest temperature of the present experiments (Table 1, Fig. 1). However, careful analysis of the data reveals that below $\sim$50 K, the diffraction peaks suddenly shift to higher angles, implying an anomalous shrinkage of the unit cell size ($-\Delta V/V_0 = 0.463(9)\%$) in a similar fashion to the response established before for $Rb_xCs_{3-x}C_{60}(x \geq 0.35)$ phases lying on the same side of the electronic phase diagram.[25] No changes in relative peak width and intensity are apparent with temperature and the observed anomalous structural response is not accompanied by a phase transition to a structure with different crystal symmetry, as confirmed by Rietveld analysis of the diffraction profiles. Figure 2 collects together data for the temperature evolution of the unit cell metrics of fcc Cs_3C_{60} and

Table 1. Refined parameters for the fcc $Rb_{0.25}Cs_{2.75}C_{60}$ phase [space group $Fm\bar{3}m$, phase fraction refined to 78.14(4)%] obtained from the Rietveld analysis of the synchrotron X-ray powder diffraction data collected at 15 K [$\lambda = 0.35420$ Å]. Estimated errors in the last digits are given in parentheses. Further details about the refinement procedures are given in Ref. 25. The weighted-profile and expected R-factors are $R_{wp} = 6.95\%$ and $R_{exp} = 4.87\%$, respectively. The lattice constant and unit cell volume are: $a = 14.60530(5)$ Å and $V = 3115.52(3)$ Å^3.

	x/α	y/b	z/c	N	B_{iso} (Å^2)
Rb	0.25	0.25	0.25	0.125	0.32(2)
Cs(1)	0.25	0.25	0.25	0.875	0.32(2)
Cs(2)	0.5	0.5	0.5	1.0	1.57(3)
C(1)	0	0.0487	0.2361	0.5	0.156(5)
C(2)	0.2061	0.0787	0.0971	0.5	0.156(5)
C(3)	0.1759	0.1572	0.0487	0.5	0.156(5)

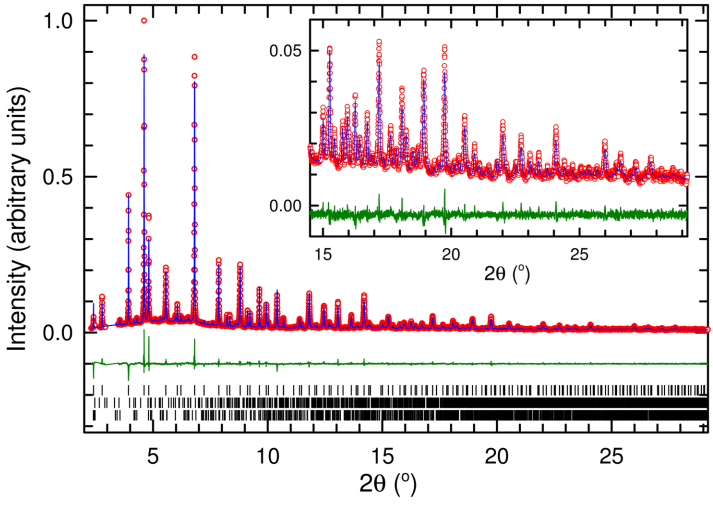

Fig. 1. (Color online) Final observed (red circles) and calculated (blue solid line) synchrotron X-ray ($\lambda = 0.35420$ Å) powder diffraction profiles for the $Rb_{0.25}Cs_{2.75}C_{60}$ sample at 15 K. The lower green solid line shows the difference profiles and the tick marks show the reflection positions of fcc $Rb_{0.25}Cs_{2.75}C_{60}$ [top], CsC_{60} [middle], and Cs_4C_{60} [bottom] phases. The inset shows an expanded view of the diffraction profile at high Bragg angles.

$Rb_xCs_{3-x}C_{60}(x = 0.25, 0.5, 1)$ with the distinct lattice collapse clearly illustrated in the $Rb_xCs_{3-x}C_{60}$ phases — its onset, T' shifts to higher temperatures as the lattice contracts with increasing Rb content, x.

Bulk superconductivity of the $Rb_{0.25}Cs_{2.75}C_{60}$ composition is confirmed by low-field magnetization measurements, M (10 Oe) [Fig. 3(a)]. The critical temperature, T_c (shielding fraction $\sim 50\%$) in overexpanded $Rb_{0.25}Cs_{2.75}C_{60}$ is 25.9 K, continuing the trend of decreasing T_c with lattice expansion on the overexpanded side of the superconductivity dome towards the Mott insulator boundary — the lowest T_c had been observed before for the $Rb_{0.35}Cs_{2.65}C_{60}$ composition at 26.9 K.[25]

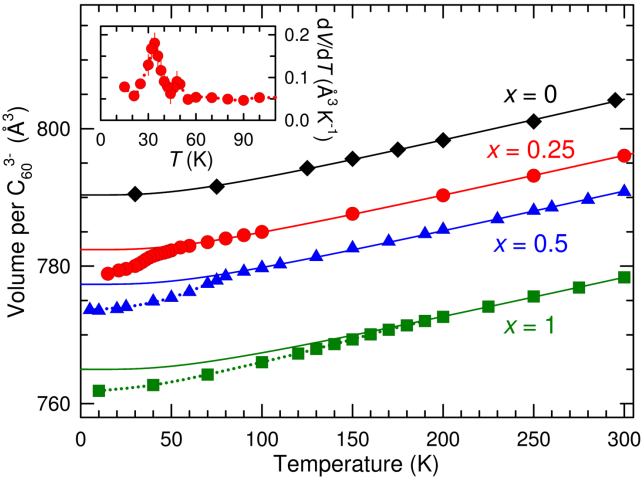

Fig. 2. (Color online) Temperature dependence of the C_{60} packing density, V, for $Rb_xCs_{3-x}C_{60}$ ($0 \leq x \leq 1$). The solid lines through the data are Debye–Grüneisen fits (for $T > T'$). The dotted lines at $T < T'$ are guides to the eye. Data for compositions with $x = 0$, 0.5 and 1 are from Refs. 8 and 25. Inset: Temperature dependence of the rate of change of V with T, dV/dT for $Rb_{0.25}Cs_{2.75}C_{60}$ clearly showing the onset of the lattice anomaly on cooling below $T' \sim 50$ K.

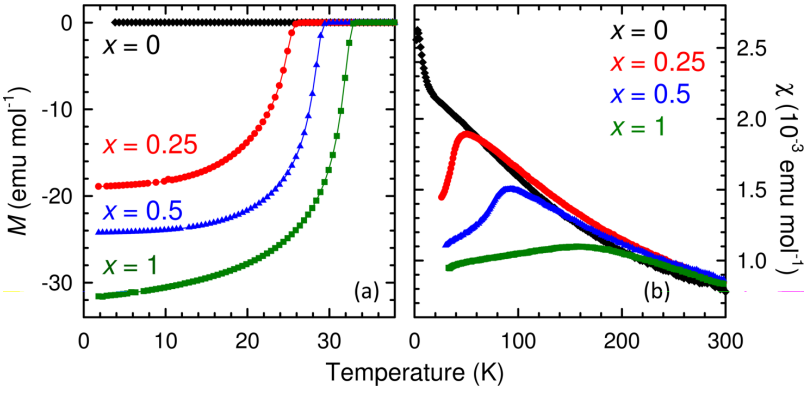

Fig. 3. (Color online) (a) Temperature dependence of the magnetization, M (10 Oe, ZFC) for the overexpanded fcc-structured $Rb_xCs_{3-x}C_{60}$ ($0 \leq x \leq 1$) compositions, showing the monotonically decreasing T_c with lattice expansion before the onset of the transition to the MJT insulator. (b) Temperature dependence of the magnetic susceptibility, $\chi(T)$, of $Rb_xCs_{3-x}C_{60}$ compositions. Data for compositions with $x = 0$, 0.5 and 1 are from Refs. 8 and 25.

Figure 3(b) shows the temperature dependence of the paramagnetic susceptibility, χ of $Rb_{0.25}Cs_{2.75}C_{60}$ together with those of fcc Cs_3C_{60} and $Rb_xCs_{3-x}C_{60}$ ($x = 0.5$, 1), measured before.[8,25] At high-temperatures, $\chi(T)$ follows the Curie–Weiss law with a negative Weiss temperature (–95(1) K) and an effective magnetic moment per C_{60}^{3-}, $\mu_{\text{eff}} = 1.645(3)\mu_B$, comparable to those in the insulating parent material, Cs_3C_{60} throughout the temperature range and in the insulating state of

the $Rb_xCs_{3-x}C_{60}$ ($x = 0.5$, 1) compositions at high temperature. This provides good evidence that $Rb_{0.25}Cs_{2.75}C_{60}$ also adopts a localized electron ground state with $S = 1/2$ per C_{60}^{3-} unit and strong antiferromagnetic correlations at high temperatures. Moreover, contrary to Cs_3C_{60}, which remains insulating in the whole temperature range but in analogy with the behavior of $Rb_xCs_{3-x}C_{60}$ ($x = 0.5$, 1), $\chi(T)$ of $Rb_{0.25}Cs_{2.75}C_{60}$ shows a well-defined cusp at $\sim$45 K on cooling — below this temperature, which closely coincides with the temperature, T' at which the lattice anomaly occurs, the susceptibility rapidly decreases until the temperature reaches T_c and the transition to the superconducting state occurs. The similarity in structural and electronic response to that established for the $Rb_xCs_{3-x}C_{60}$ ($x \geq 0.35$) compositions before suggests that both the susceptibility cusps and the concurrently occurring lattice collapse in $Rb_{0.25}Cs_{2.75}C_{60}$ on cooling also signify insulator-to-metal crossover driven by the reduced bandwidth which accompanies the lattice contraction induced by temperature. This is consistent with the negative volume change, $\Delta V = V_M - V_I$, across the transition (Fig. 2), as virial theorem analysis of the metal-to-insulator (M–I) transition assigns itinerant electrons a lower volume. The extended electronic phase diagram of fcc A_3C_{60} fullerides to include the additional information derived by the present experiments on the $Rb_{0.25}Cs_{2.75}C_{60}$ composition, which lies closer to the MJT insulator boundary than ever achieved before is drawn in Fig. 4.

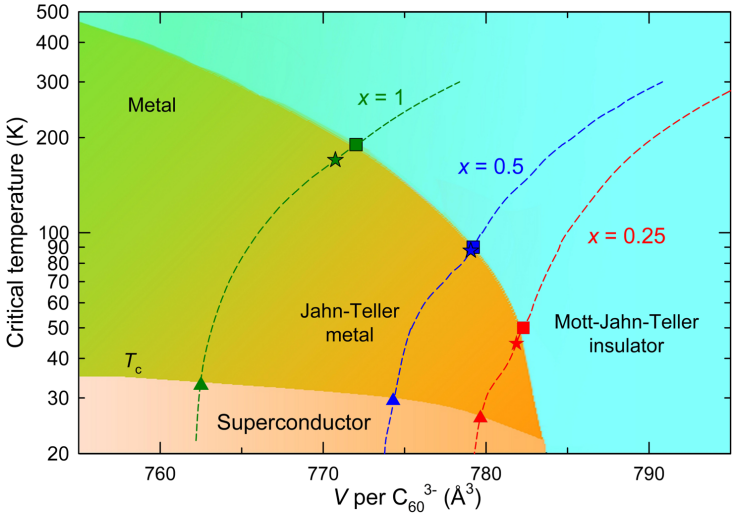

Fig. 4. (Color online) Updated electronic phase diagram of fcc $Rb_xCs_{3-x}C_{60}$ in the overexpanded region showing the evolution of T_c (solid triangles) and the MJTI-to-JTM crossover temperature, T' (synchrotron X-ray powder diffraction: Squares; magnetic susceptibility: stars) as a function of packing density, V. Within the metallic (superconducting) regime, gradient shading from orange to green schematically illustrates the JTM to conventional metal (unconventional to weak-coupling BCS conventional superconductor) crossover. Dashed lines mark experimental $V(T)$ tracks for selected $Rb_xCs_{3-x}C_{60}$ ($x = 0.25$, 0.5, 1) compositions.

4. Conclusion

A_3C_{60} molecular superconductors share a common electronic phase diagram with unconventional high-temperature superconductors such as the cuprates. However, unlike atom-based superconductors, the antiferromagnetic Mott insulating state out of which superconductivity emerges is controlled by the C_{60}^{3-} molecular electronic structure via the on-molecule Jahn–Teller effect influence on molecular geometry and spin state. We have established before that chemical and/or physical pressurization, which tunes the bandwidth quasi-continuously, leads to the destruction of the parent MJT insulating state and yields an anomalous metallic state (termed Jahn–Teller metal) where quasi-localized and itinerant electron behavior co-exist.[25] This poor metallic state is the parent state of the highest T_c superconductor.

Here, we have extended the compositional range of experimentally accessible superconducting fcc-structured $Rb_xCs_{3-x}C_{60}$ phases through solid state routes to the lowest Rb content, $x = 0.25$ ever achieved, i.e., affording more expanded fcc phases and approaching closely the MJT insulator boundary. At ambient pressure, the $Rb_{0.25}Cs_{2.75}C_{60}$ composition is insulating at high-temperature and crosses over into the Jahn–Teller metallic state below $\sim$45–50 K, as indicated by synchrotron powder X-ray diffraction and magnetic susceptibility measurements. Further cooling leads to the emergence of a bulk superconductor (shielding fraction $\sim$50%) with a T_c onset of 25.9 K, the lowest ambient pressure T_c recorded for any A_3C_{60} fulleride before the transition to the MJT insulating state adopted by Cs_3C_{60}. We note, however, that even for the most expanded $Rb_{0.25}Cs_{2.75}C_{60}$ composition accessed here, there are no signs of phase coexistence between the insulating and metallic phases in all experimental datasets as the transition is traversed upon cooling. As the Mott transition is of first order, a phase coexistence regime ending at a critical point in the volume–temperature phase diagram is expected,[30,31] in analogy with the liquid–gas transition. Its absence here implies that the critical temperature for the Mott transition is lower than 45 K with $Rb_{0.25}Cs_{2.75}C_{60}$ lying still in the supercritical region of the electronic phase diagram. Therefore, further effort to fine-tune the synthetic techniques to afford fcc-structured $Rb_xCs_{3-x}C_{60}$ with values of the Rb content, x even smaller than 0.25 is needed. This will ensure success in approaching the M–I boundary even closer and encountering the first-order Mott line, which should be located between $x = 0$ and 0.25. Past work in this direction is encouraging with evidence of phases with x as small as 0.12 being accessible.[32]

Acknowledgments

This work was sponsored by the World Premier International (WPI) Research Center Initiative for Atoms, Molecules and Materials, Ministry of Education, Culture, Sports, Science and Technology of Japan. We acknowledge the financial support from the Mitsubishi Foundation and the Japan Society for the Promotion of Science (JSPS) under the Scientific Research on Innovative Areas 'J-Physics' (No. JP15H05882) and 'π-System Figuration' (JP17H05139) Projects. We thank

the ESRF for the access to synchrotron X-ray facilities and Prof. A.N. Fitch for the help with the synchrotron XRD experiments.

References

1. G. Zhao, *Phys. Scr.* **83**, 038302 (2011).
2. M. R. Norman, *Science* **332**, 196 (2011).
3. P. A. Lee *et al.*, *Rev. Mod. Phys.* **78**, 17 (2006).
4. Y. J. Uemura, *Nat. Mater.* **8**, 253 (2009).
5. Q. Si and F. Steglich, *Science* **329**, 1161 (2010).
6. A. Y. Ganin *et al.*, *Nat. Mater.* **7**, 367 (2008).
7. Y. Takabayashi *et al.*, *Science* **323**, 1585 (2009).
8. A. Y. Ganin *et al.*, *Nature* **466**, 221 (2010).
9. Y. Ihara *et al.*, *Phys. Rev. Lett.* **104**, 256402 (2010).
10. A. Potocnik *et al.*, *Chem. Sci.* **5**, 3008 (2014).
11. A. Potocnik *et al.*, *Sci. Rep.* **4**, 4265 (2014).
12. P. Wzietek *et al.*, *Phys. Rev. Lett.* **112**, 066401 (2014).
13. Y. Kasahara *et al.*, *Phys. Rev. B* **90**, 014413 (2014).
14. J. E. Han *et al.*, *Phys. Rev. Lett.* **90**, 167006 (2003).
15. G. R. Darling *et al.*, *Phys. Rev. Lett.* **101**, 136404 (2008).
16. M. Capone *et al.*, *Rev. Mod. Phys.* **81**, 943 (2009).
17. R. Akashi and R. Arita, *Phys. Rev. B* **88**, 054510 (2013).
18. Y. Murakami *et al.*, *Phys. Rev. B* **88**, 125126 (2013).
19. Y. Nomura *et al.*, *Sci. Adv.* **1**, e1500568 (2015).
20. H.-C. Jiang and S. Kivelson, *Phys. Rev. B* **93**, 165406 (2016).
21. N. Iwahara and L. F. Chibotaru, *Nat. Commun.* **7**, 13093 (2016).
22. G. Klupp *et al.*, *Nat. Commun.* **3**, 912 (2012).
23. K. Kamarás *et al.*, *J. Phys. Conf. Ser.* **428**, 012002 (2013).
24. E. Fradkin and S. A. Kivelson, *Nat. Phys.* **8**, 864 (2012).
25. R. H. Zadik *et al.*, *Sci. Adv.* **1**, e1500059 (2015).
26. S. Hoshino and P. Werner, *Phys. Rev. Lett.* **118**, 177002 (2017).
27. P. Werner *et al.*, *Phys. Rev. B* **95**, 195405 (2017).
28. Y. Kasahara *et al.*, *Nat. Commun.* **8**, 14467 (2017).
29. A. C. Larson and R. B. von Dreele, GSAS software, Los Alamos National Laboratory Report No. LAUR 86-748 (2000).
30. A. Jayaraman *et al.*, *Phys. Rev. B* **2**, 3751 (1970).
31. F. Kagawa *et al.*, *Nat. Phys.* **5**, 880 (2009).
32. M. T. McDonald, PhD Thesis, Durham University (2010).